Dynamic Processes of 1,1′-Dihydroxy-2,2′,6,6′-tetra-*tert*-butylbiphenyl Radical Cation in Sulfuric Acid As Studied by Two-Dimensional FT-EPR Spectroscopy

S. Kababya,[†] I. Bilkis,[‡] and D. Goldfarb*[,†]

Contribution from the Department of Chemical Physics, Weizmann Institute of Science, 76100 Rehovot, Israel, and Institute of Biochemistry, Food Science and Nutrition, Faculty of Agriculture, Hebrew University, Rehovot, Israel

Received March 7, 1996[⊗]

Abstract: Slow exchange processes in the solution of the 1,1′-dihydroxy-2,2′,6,6′-tetra-*tert*-butylbiphenyl cation radical (tBBP$^{\bullet+}$) in concentrated sulfuric acid were investigated by two-dimensional (2D) exchange FT-EPR spectroscopy (EXSY) in the temperature range of 281−310 K. The radical was obtained by dissolving 2,2′,6,6′-tetra-*tert*-butyldiphenoquinone (tBDP) in concentrated sulfuric acid. The EPR spectrum of the radical cation, tBBP$^{\bullet+}$, showed that the four aromatic protons and the two hydroxyl protons are magnetically equivalent. The 2D EXSY spectra exhibited cross peaks between hyperfine components with $\Delta M_I^a = \pm 1$ and $\Delta M_I^b = \pm 1$, where a and b correspond to the aromatic and hydroxyl protons, respectively. Based on this selective cross-peak pattern, the change in the nuclear quantum number of the aromatic protons was attributed to proton spin−lattice relaxation. In contrast, the change in the nuclear quantum number of the hydroxyl protons could arise from proton exchange with the solvent and/or nuclear spin−lattice relaxation. Temperature-dependent measurements showed that the intensity of the cross peaks decreased with increasing temperatures, indicating that in the case of the hydroxyl protons the cross peaks are also a consequence of nuclear relaxation and not proton exchange. The nuclear spin−lattice relaxation rates of the two types of protons and the electron spin−lattice relaxation, T_1, were determined from simulations of experimental 2D spectra recorded with different mixing times. The values obtained at 291 K were $T_{1a}^{-1} = (9 \pm 1) \times 10^5\ s^{-1}$ and $T_{1b}^{-1} = (4 \pm 1) \times 10^5\ s^{-1}$ and $T_1 = (0.83 \pm 0.06) \times 10^5\ s^{-1}$. Using the nuclear relaxation rate of the aromatic protons and assuming that the nuclear relaxation is dominated by the hyperfine anisotropy mechanism, a correlation time of 0.67×10^{-9} s was obtained. This value was further used to account for the M_I dependence of the line width. Similar temperature-dependent 2D EXSY measurements were carried out on the dihydroduroquinone radical cation in sulfuric acid. In this case, the cross peaks observed were attributed to both proton exchange and nuclear spin relaxation of the hydroxyl protons. The proton exchange in the dihydroduroquinone radical cation was faster than in tBBP$^{\bullet+}$.

Introduction

Two-dimensional (2D) exchange FT-EPR spectroscopy (EXSY) is an effective tool for investigating slow dynamic processes of organic radicals in solutions. Although a relatively small number of 2D EXSY studies have been reported so far, they cover a variety of processes including Heisenberg exchange,[1−6] electron transfer,[7] cation hopping in ion pairs,[8,9] photoinduced proton abstraction,[10] proton exchange,[11] and nuclear relaxation.[3,12−14] All these processes cause changes in the hyperfine coupling and/or the nuclear spin states of coupled nuclei, which are manifested in the appearance of cross peaks between selected hyperfine components in the 2D spectrum. These cross peaks readily identify the nuclear states that are mixed by the dynamic process and thus provide "finger prints" for the exchange mechanism. This is in contrast to the conventional method of line shape analysis where an exchange model is first assumed and then validated by computer simulations which reproduce the temperature dependence of the line shape. The 2D EXSY method also allows the detection and determination of the rates of simultaneously occurring dynamic processes, provided that they exhibit different cross-peak patterns.[9] However, it may happen that coexisting dynamic processes generate the same pattern of cross peaks. In this case, the deconvolution of the processes requires variations of the temperature or composition of the sample under study. In this

[†] Weizmann Institute.
[‡] Hebrew University.
[⊗] Abstract published in *Advance ACS Abstracts,* September 1, 1996.

(1) Millhauser, G. L.; Gorcester, J.; Freed, J. H. In *Electronic Magnetic Resonance of the Solid State*; Weil, J. A., Ed.; Canadian Society for Chemistry: Ottawa, Canada, 1987.
(2) Gorcester, J.; Freed, J. H. *J. Chem. Phys.* **1986**, *85*, 5375.
(3) Gorcester, J.; Rananvare, S.; Freed, J. H. *J. Chem. Phys.* **1989**, *90*, 5764.
(4) Gorcester, J.; Millhauser, G. L.; Freed, J. H. *Advanced EPR;* Hoff, A. J., Ed.; Elsevier: Amsterdam, 1989.
(5) Gorcester, J.; Millhauser, G. L.; Freed, J. H. In *Modern Pulsed and Continuous Wave Electron Spin Resonance*; Kevan, L., Bowman, M. K., Eds.; John Wiley and Sons: New York, 1990; p 119.
(6) Freed, J. H. *J. Chem. Soc., Faraday Trans.* **1990**, *86*, 3173.
(7) Angerhofer, A.; Massoth, R. J.; Bowman, M. K. *Isr. J. Chem.* **1988**, *28*, 227.
(8) Fauth, J. M.; Kababya, S.; Goldfarb, D. *J. Magn. Reson.* **1991**, *92*, 203.
(9) Kababya, S.; Luz, Z.; Goldfarb, D. *J. Am. Chem. Soc.* **1994**, *116*, 5805.
(10) Pulschau, M.; Dinse, K. P. *J. Magn. Reson.* **1994**, *109*, 181.
(11) Weber, R. T., Bruker Application Note, 1994.
(12) Rübsam, M.; Plüschau, M.; Schweitzer, P.; Dinse, K.-P.; Fuchs, D.; Rietschel, H.; Michel, R. H.; Benz, M.; Kapps, M. M. *Chem. Phys. Lett.* **1995**, *240*, 615.
(13) Lee, S.; Patyal, B. R.; Saxena, S.; Crepeau, R. H.; Freed, J. H. *Chem. Phys. Lett.* **1994**, *221*, 397.
(14) Crepeau, R. H.; Saxena, S.; Lee, S. L.; Patyal, B.; Freed, J. H. *Biophys. J.* **1994**, *66*, 1489.

S0002-7863(96)00737-8 CCC: $12.00

work, we present a case that falls within this category. The processes involved are proton exchange and nuclear spin−lattice relaxation in 1,1′-dihydroxy-2,2′,6,6′-tetra-*tert*-butylbiphenyl radical cation (tBBP$^{\bullet+}$, **I**) in concentrated sulfuric acid.

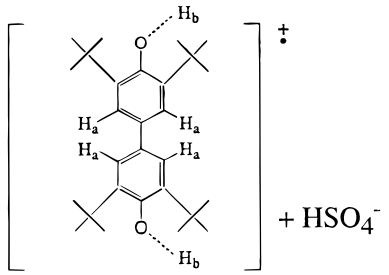

I

The cation hopping in ion pairs of the radical anion of 2,2′,6,6′-tetra-*tert*-butyldiphenoquinone (tBDP) with alkali metal cations was investigated by continuous wave (CW) EPR, and rate constants were determined for different cations and solvents.[15] The dynamic processes in solutions of the radical cation of tBBP$^{\bullet+}$ have, however, not yet been studied. Two possible chemical exchange processes can be envisioned, the cis−trans isomerization of the hydroxyl groups and the exchange of the hydroxyl protons with the protons of the solvent, H_2SO_4 in our case. Cis−trans isomerization have been observed in several dihydroquinone cation radicals.[16,17] In the dihydroduroquinone cation radical (DQ$^{\bullet+}$), the rotation of the hydroxyl groups about the C−O bonds modulates the hyperfine couplings of the methyl protons and a line shape analysis gave mechanistic details and rates.[16] The proton exchange process in DQ$^{\bullet+}$ has been found to be significantly slower than the cis−trans isomerization of the hydroxyl groups, and it was studied for the first time by 2D EXSY at a temperature where the cis−trans isomerization is fast.[11] The exchange of the hydroxyl protons with solvent protons leads to a mixing of all possible nuclear spin states of the hydroxyl protons and therefore is expected to generate cross peaks between all hyperfine components with different M_I^{OH}, i.e., among all hyperfine lines of the hydroxyl triplets. But because the process is slow, the probability of an exchange of the two hydroxyl protons during the mixing time is relatively low and cross peaks were observed only between hyperfine lines corresponding to $\Delta M_I^{OH} = \pm 1$, where I corresponds to the total spin of the hydroxyl protons.

In addition to the two chemical exchange processes described above, selective mixing of hyperfine components can occur due to nuclear spin−lattice relaxation. When the latter is comparable or shorter than the spin−lattice relaxation of the radical, T_1, a change in the spin state of any of the nuclei may take place during the mixing time. At relatively short mixing times, the nuclear relaxation mixes only hyperfine lines within a multiplet of a group of magnetically equivalent nuclei with the selection rules of $\Delta M_I = \pm 1$.[3] At long mixing times, the probability of consecutive flips of two nuclear spins, corresponding to a total change of $\Delta M_I = \pm 2$, may become significant.[14] Likewise, the probability of a flip of two nuclei belonging to different groups increases as well. Note that the same cross-peak pattern is generated by the nuclear relaxation of the hydroxyl protons and their exchange with solvent protons. Another mechanism that may lead to cross peaks in this particular system is the Heisenberg exchange. Unlike the mechanisms discussed above, the Heisenberg exchange is nonelective and results in the appearance of cross peaks between all hyperfine components.[1]

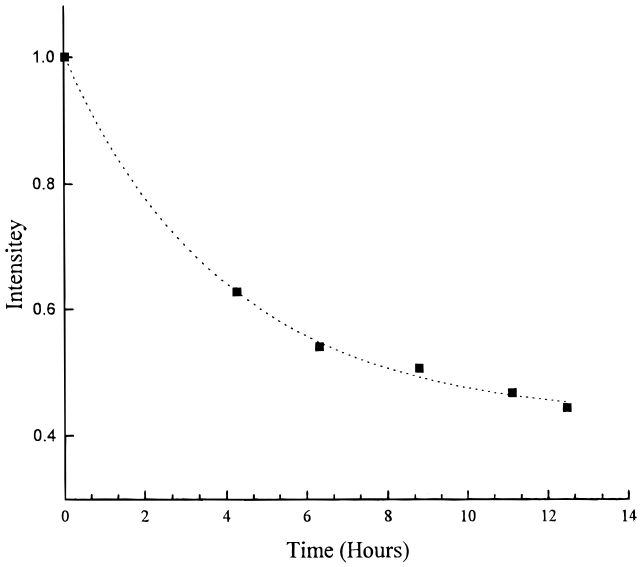

Figure 1. Intensity of the FT-EPR spectrum of tBBP$^{\bullet+}$ as a function of time ($t = 0$ corresponds to beginning of the first 2D experiment).

Three types of measurements are presented in this work: CW-EPR, one-dimensional (1D) FT-EPR, and 2D EXSY. Temperature-dependent CW-EPR measurements were essential for peak assignment, for establishing that the rate of the exchange process was indeed within the slow limit, and for line width determination. The latter was required for the quantitative analysis of the 2D EXSY spectra. Due to technical difficulties such as spectrometer dead time and bandwidth limitations, the relative amplitudes of the peaks in the FT-EPR and the CW-EPR spectra may be different. Therefore, any possible distortion of the FT-EPR spectrum had to be understood and accounted for prior to a quantitative analysis of the 2D spectrum. The temperature-dependent 2D EXSY measurements showed that the cross peaks observed are a consequence of relatively fast nuclear spin−lattice relaxation of both the aromatic and the hydroxyl protons. Furthermore, the exchange of the hydroxyl protons was too slow at ambient temperatures and could not be detected by the 2D EXSY method. Similar temperature-dependent 2D EXSY measurements that were performed on DQ$^{\bullet+}$ in sulfuric acid showed that the previously determined rates of the proton exchange[11] contained a significant contribution from the nuclear relaxation of the hydroxyl protons.

Experimental Section

Radicals Preparation. The cation radical was prepared by dissolving tBDP, prepared for us by Synthos, in concentrated sulfuric acid (H_2SO_4 or D_2SO_4, Aldrich). The concentration of tBDP was 1 mM. Sodium dithionite ($Na_2S_2O_4$) was added to minimize the production of the dication, and oxygen was removed from the solution by bubbling in dry nitrogen for 15 min with stirring. The deep purple solution was then placed in a capillary glass tube (∼1 mm o.d.), additional degassing was carried out on a vacuum line to ensure the complete removal of oxygen, and the sample tube was then sealed. In spite of all these precautions, tBBP$^{\bullet+}$ was unstable at room temperature and it lost within 4 h 45% of its EPR intensity. The decay of the tBBP$^{\bullet+}$ concentration was followed by measurement of the FT-EPR spectrum before and after each 2D experiment, as shown in Figure 1. Two-dimensional measurements were performed within a few days from the sample preparation. The samples were stored in liquid nitrogen until the measurements were performed. If in the course of a series of experiments the signal became too weak, the sample was replaced with a new sample prepared under the same conditions. DQ$^{\bullet+}$ was prepared as tBBP$^{\bullet+}$.

(15) Prokof'ev, A. I.; Solodovnikov, S. P.; Volod'kin, A. A.; Ershov, V. V.; Kabachnik, M. I. *Izv. Akad. Nauk SSSR, Ser. Khim.* **1973**, 2403.
(16) Bolton, J. R.; Carrington, A. *Mol. Phys.* **1962**, *5*, 161.
(17) Carrington, A. *Mol. Phys.* **1962**, *4*, 25.

Table 1. Phase Cycle Used in the EXSY Experiments[a]

file I (cos $\omega t_1 e^{i\omega t_2}$)				file II (sin $\omega t_1 e^{i\omega t_2}$)			
φ_1	φ_2	φ_3	R	φ_1	φ_2	φ_3	R
X	X	X	X	X	Y	Y	−X
X	−X	X	−X	X	−Y	Y	X
X	X	−X	−X	X	Y	−Y	X
X	−X	−X	X	X	−Y	−Y	−X
X	X	Y	Y	X	Y	−X	−Y
X	−X	Y	−Y	X	−Y	−X	Y
X	X	−Y	−Y	X	Y	X	Y
X	−X	−Y	Y	X	−Y	X	−Y

[a] φ_1, φ_2, and φ_3, correspond to the phase of the first, second, and third pulses and R corresponds to the receiver phase. The data are saved in two files, I and II.

Two-dimensional EXSY spectra of tBBP$^{\bullet+}$ in sulfuric acid with and without $Na_2S_2O_4$ showed no differences, indicating that $Na_2S_2O_4$ does not take part in any of the dynamic processes detected by the 2D experiment.

Spectroscopic Measurements. CW-EPR measurements (∼9 GHz) were performed on a Varian E12 spectrometer interfaced to a personal computer and equipped with variable temperature accessories. The pulsed EPR experiments were carried out on a home built spectrometer operating at ≈9.2 GHz.[18] One-dimensional FT-EPR spectra were recorded in quadrature using the CYCLOP phase cycle,[19] and the pulse sequence employed for the 2D experiments was $(\pi/2)_{\varphi_1} - t_1 - (\pi/2)_{\varphi_2} - \tau_m - (\pi/2)_{\varphi_3} - t_2$. The width of the $\pi/2$ pulses was 14 ns, and the resulting FID was collected in quadrature using a 16-step phase cycle given in Table 1. This phase cycle allows quadrature detection in both dimensions, and it eliminates axial peaks and quadrature images.[9,20,21] The data corresponding to the cos $\omega_i t_1 e^{\omega_j t_2}$ and sin $\omega_i t_1 e^{i\omega_j t_2}$ signals were collected in two separate files as listed in Table 1, and the data were treated as described previously.[9]

In all experiments, the dwell time was 20 ns in both t_1 and t_2, the number of points in t_1 and t_2 were 60 × 130 for tBBP$^{\bullet+}$ and 170 × 350 for DQ$^{\bullet+}$, and between 500 and 1000 FIDs were accumulated for each t_1 value. The mixing time, τ_m, was varied between 0.3 and 6.0 μs, and the repetition rate was 100 Hz. Usually, the dead time was 160 ns in t_2 and 80 ns in t_1, but in the case of the tBBP$^{\bullet+}$ samples, the effective dead time in the 2D experiment was found to be longer (220 ns). The reason is the reduced S/N due to the low stability of the radical, which required short acquisition times and therefore did not allow long accumulations. The dead time in t_1 originated from the limited speed of the phase shifter.

Data Manipulation. The 2D spectra are presented in the "anti echo", magnitude mode, which is obtained by the addition of the two files listed in Table 1 prior to Fourier transformation.[9,20,21] This procedure results in a main diagonal stretching from top left to bottom right. Prior to Fourier transformation, bad data points due to spectrometer dead time were removed, baseline correction was applied, and zero filling to a 256 × 256 matrix for tBBP$^{\bullet+}$ and 512 × 512 matrix for DQ$^{\bullet+}$ was performed. The resulting time domain matrix was then convoluted with a sine bell function in both dimensions and a 2D FT was carried out.

The overlap of the cross peaks with the tails of the intense diagonal peaks, and the lower resolution of amplitude-mode spectra with respect to phase-sensitive spectra, make the determination of the volume integrals of cross peaks difficult. It is therefore more convenient to express the results in terms of peak amplitudes, which is acceptable if all peaks have the same width.[20,22] The cases of tBBP$^{\bullet+}$ and DQ$^{\bullet+}$ in sulfuric acid, however, do not fall within this category. Therefore, the peak amplitudes can serve only for the comparison of the intensity of the same peak as a function of τ_m. The amplitudes of the peaks were determined by selecting for each diagonal peak cross sections along the ω_1 and ω_2 dimensions, generating 1D spectra, and the peak heights were determined by applying proper baseline and overlap corrections.

Simulated time domain spectra data were manipulated as the experimental data; points within the dead times were removed and the time domain traces were multiplied by a decaying exponent in t_1 to account for decay of the radical during the 2D measurement. Finally the relative intensities of the various peaks in the spectra were adjusted to account for the spectrometer bandwidth (or coverage), which depends on the pulse width and on the resonator bandwidth. The spectrometer bandwidth was determined by measuring the FT-EPR spectrum of perdeuterated (PD) tempone in toluene-d_8 as a function of the magnetic field, holding the spectrometer frequency constant.[14] The calculated spectra were multiplied by this coverage profile.

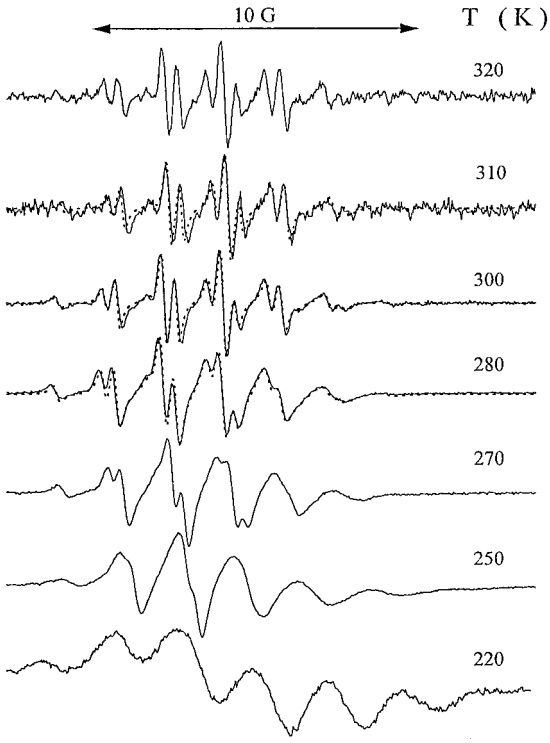

Figure 2. CW-EPR spectra of tBBP$^{\bullet+}$ in H_2SO_4 recorded at different temperatures. The dotted traces represent simulated spectra with the line widths given in Table 2. The microwave power used was 2 mW, and the modulation amplitude was 0.1 G.

Results

CW-EPR Measurements of tBBP$^{\bullet+}$. The EPR spectrum of tBBP$^{\bullet+}$ in H_2SO_4 recorded at 320 K, is shown in Figure 2. It consists of a total of 15 lines arising from a quintet due to the four aromatic protons ($|a_H^a| = 1.81$ G (5.07 MHz)), which is further split into triplets by the two hydroxyl protons ($|a_H^b| = 1.42$ G (3.98 MHz)). This assignment was confirmed by the preparation of the radical in D_2SO_4, where the hydroxyl triplets were replaced with quintets with a reduced splitting, $|a_D^b| = 0.24$ G (0.67 MHz), due to the two ^{2}H nuclei. The EPR spectra show that the ring protons are equivalent, indicating that either the cis−trans isomerization is fast or it does not affect the hyperfine coupling of the aromatic protons because they are sufficiently far from the hydroxyl groups.

The EPR spectra recorded in the temperature range 220−320 K, presented in Figure 2, showed that as the temperature decreased, the line widths increased and the spectra became highly asymmetric. Likewise, asymmetric broadening was also observed in the EPR spectrum of tBBP$^{\bullet+}$ in D_2SO_4. The variation in line width throughout the spectrum is caused by

(18) Goldfarb, D.; Fauth, J. M.; Tor, Y.; Shanzer, A. *J. Am. Chem. Soc.* **1991**, *113*, 1941.
(19) Hoult, D. I.; Richards, R. E. *Proc. R. Soc. London, Ser. A* **1975**, *344*, 311.
(20) Gorcester, J.; Freed, J. H. *J. Chem. Phys.* **1988**, *88*, 4678.
(21) States, D. J.; Haberkon, R. A.; Ruben, D. J. *J. Magn. Reson.* **1982**, *48*, 286.
(22) Orekhov, V. Yu.; Barsulov, T. L.; Barsukov, I. L.; Pervishin, K. N.; Aiseniev, A. S. *Appl. Magn. Reson.* **1992**, *3*, 965.

Table 2. Line Widths, ΔH (in gauss), of the EPR Lines of tBBP$^{\bullet+}$ in H_2SO_4[a]

peak no.	$M_{Ia}M_{Ib}$	ΔH 310 *K*	300 *K*	280 *K*
15	−2, −1	0.178	0.179	0.22
14	−2, 0	0.152	0.163	0.211
13	−1, −1	0.174	0.164	0.22
12	−2, +1	0.181	0.179	0.271
11	−1, 0	0.164	0.202	0.245
10	0, −1	0.172	0.164	0.237
9	−1, +1	0.177	0.169	0.271
8	0, 0	0.179	0.187	0.297
7	+1, −1	0.174	0.186	0.271
6	0, +1	0.208	0.194	0.357
5	+1, 0	0.198	0.225	0.365
4	+2, −1	0.213	0.227	0.391
3	+1, +1	0.245	0.272	0.46
2	+2, 0	0.220	0.283	0.451
1	+2, +1	0.249	0.328	0.511

[a] The widths were determined from simulations of the CW-EPR spectra at different temperatures using eq. 1. The peaks are numbered successively from high to low fields.

relaxation mechanisms which depend on the magnetic quantum numbers of the nuclei in the molecule.[23] The explicit dependence of the transverse relaxation rate, T_2^{-1}, on M_I in the case of two groups of magnetically equivalent nuclei, *a* and *b*, is [23,24]

$$T_2^{-1} = a + b_a M_{Ia} + b_b M_{Ib} + c_a M_{Ia}^2 + c_b M_{Ib}^2 + dM_{Ia}M_{Ib} \quad (1)$$

and the line width, ΔH, is related to T_2, according to

$$T_2^{-1} = \sqrt{3}(2.8 \times 10^6)\pi\Delta H \text{ s}^{-1} \quad (2)$$

Our system does not fully comply with the requirements for which eq 1 holds since the group of the aromatic protons consists of two subgroups of completely equivalent protons. In this case, each EPR line is composed of a superposition of several Lorentzian lines with different widths and the line shape of the composite line is not necessarily Lorentzian.[23] A rigorous analysis thus requires the diagonalization of the relaxation matrix.[23] However, in many instances, including our case, experimental limitations make it impossible to differentiate the predicted non-Lorentzian shape of the composite lines from the actual line shape.[23] Therefore, we assumed that all aromatic protons are completely equivalent and eq 1 can be used for the determination of the line widths of the various hyperfine components. As will be shown later, the line widths are essential parameters for the determination of the rate constants by simulations of 2D EXSY spectra.

The line width of each line was initially estimated from the experimental spectrum and then refined by simulations of the EPR spectrum using eq 1 and a Lorentzian line shape. Simulated spectra appear as dotted traces in Figure 2, and Table 2 lists the ΔH values for each line in the spectra of tBBP$^{\bullet+}$ in H_2SO_4 measured at 280, 300, and 310 K. The parameters *a*, b_a, b_b, c_a, c_b, and *d*, as determined from the line widths, are given in Table 3, and their temperature dependence is shown in Figure 3. The fit of the line widths to eq 1 also yields the sign of the hyperfine coupling. Reasonable results could be obtained only with the assignment of lines as listed in Table 2, where the hyperfine coupling of both types of protons is negative as expected.

(23) Freed, J. H.; Frankel, G. K. *J. Chem. Phys.* **1963**, *9*, 326.
(24) Silver, B. L.; Luz, Z.; Eden, C. *J. Chem. Phys.* **1966**, *44*, 4421.

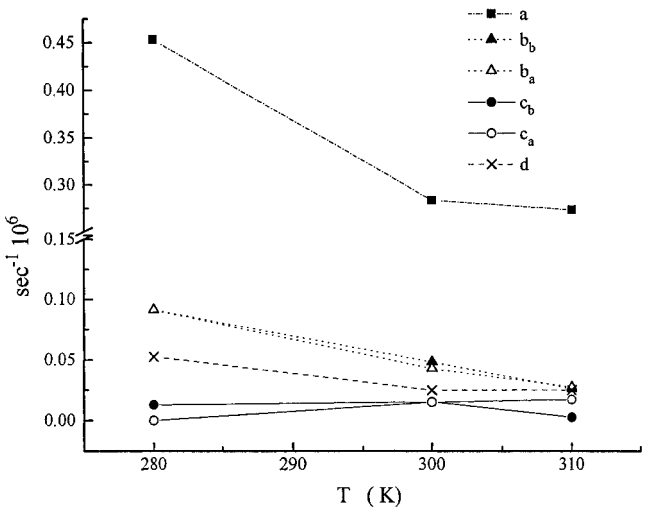

Figure 3. The temperature dependence of *a*, b_i, c_i, and *d* for tBBP$^{\bullet+}$ in H_2SO_4.

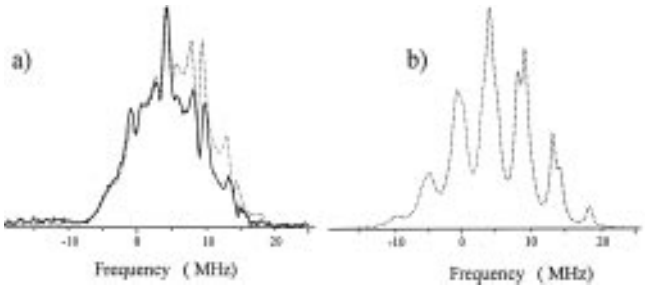

Figure 4. FT-EPR spectra of tBBP$^{\bullet+}$ in H_2SO_4 recorded at 281 K (a) experimental magnitude spectrum with 160 ns dead time (solid trace) and simulated magnitude spectrum (dotted trace) calculated by taking into account the spectrometer bandwidth and the dead time and using the line widths listed in Table 2. (b) A simulated absorption spectrum calculated with the line width listed in Table 2.

Table 3. Parameters *a*, b_a, c_a, c_b, and *d* (in 10^{-6} s^{-1}) (see eq 1) for tBBP$^{\bullet+}$ at Different Temperatures

temp (K)	*a*	b_a	b_b	c_a	c_b	*d*
310	2.73	0.26	0.27	0.027	0.17	0.25
300	2.83	0.48	0.43	0.15	0.15	0.25
280	4.53	0.91	0.91	0.13	0.0	0.52

1D FT-EPR Measurements of tBBP$^{\bullet+}$. The magnitude-mode spectrum of tBBP$^{\bullet+}$ at 298 K, obtained from the FID generated by the application of a single $\pi/2$ pulse, is shown in Figure 4a. The spectrum differs significantly from that of the integrated CW-EPR spectra shown above. Comparison with a simulated absorption spectrum, depicted in Figure 4b, calculated with the line widths listed in Table 2 and the hyperfine coupling constants $a_H^a = -1.81$ G and $a_H^b = -1.42$ G, showed that the differences are mainly the lower intensity of the outer peaks due to the limited bandwidth of the spectrometer, the dead time, and the loss of resolution arising from the magnitude-mode presentation. Once these effects are taken into account, according to the description given in the Experimental Section, the experimental spectrum could be better reproduced, as shown by the dashed trace in Figure 4a. The same types of distortions are expected in the 2D EXSY spectra, and therefore their origin had to be determined and quantified.

2D EXSY Measurements of tBBP$^{\bullet+}$. Two-dimensional spectra of tBBP$^{\bullet+}$ in H_2SO_4, recorded as a function of the mixing time, τ_m, at 291 K, are shown in Figure 5. The intensities of the cross peaks in the 2D maps depend on both τ_m and the temperature. The spectrum recorded with $\tau_m = 0.3$ μs exhibits

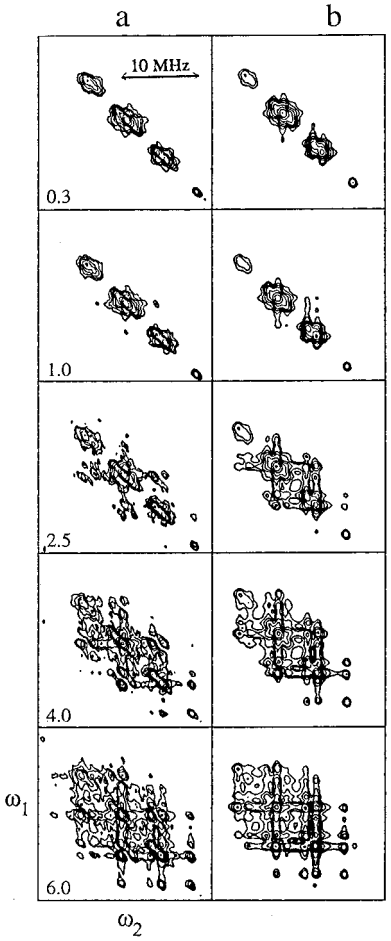

Figure 5. Experimental (a) and simulated (b) 2D EXSY contour plot spectra of $tBBP^{\bullet+}$ in H_2SO_4 measured at 291 K as a function of τ_m. The value of τ_m in μs is listed in the figure.

diagonal peaks, and out of the 15 expected peaks, only 8 are apparent. The spectrum appears asymmetric since the spectrometer dead time affects to a greater extent the peaks in the low-frequency end, which are broader than those in the high-frequency end. The spectrum recorded with $\tau_m = 1.0$ μs exhibits cross peaks at [(0, 0), (0, 1)] and [(0, 0), (0, −1)] where the numbers in brackets correspond to (M_{Ia}, M_{Ib}) as defined in Figure 6. These cross peaks represent mixing within the triplets of the hydroxyl protons. A further increase in the mixing time to $\tau_m = 2.5$ μs resulted in the appearance of additional cross peaks, showing that mixing within the quintets of the aromatic protons occurs as well.

For convenience, the labeling of the hyperfine components in the stick diagram EPR spectrum and the connectivities of the cross peaks in 2D spectra obtained with $\tau_m = 2.5$ μs at 281 and 291 K are shown in Figure 6. In this figure the diagonal peaks that correspond to (M_{Ia}, M_{Ib}) values of (0, 0), (0, −1), (−1, 0), and (−1, −1) were labeled 8, 10, 11, and 13, respectively and the cross peaks (8, 10), (8, 11), and (11, 13) were labeled as well. The peaks connected by solid lines represent mixing within the triplet, occurring due to a change in the spin state of one the hydroxyl protons, H_b, such that $\Delta M_{Ib} = \pm 1$, whereas those connected by dotted lines originate from a change in the spin state of one of the four ring protons, H_a ($\Delta M_{Ia} = \pm 1$). These connectivities are also shown on the stick diagram in the bottom of Figure 6. Figure 5a shows that up to $\tau = 2.5$ μs there is no mixing between the triplets and the quintets. At longer mixing times, 4.0 and 6.0 μs, cross peaks corresponding to a total change of $\Delta M_I = \pm 2$ become evident as well. The appearance of selected cross peaks in all of these spectra excludes the existence of Heisenberg exchange in these samples.

The 2D spectra recorded at 281 K show the same general behavior as of those recorded at 291 K. At 281 K the peaks are broader and the asymmetry of the spectrum is significantly larger. The τ_m dependence of the amplitudes of the diagonal and cross peaks in the spectra recorded at 281 K is summarized in Figure 7. The intensities of the diagonal peaks decrease with τ_m due to T_1 and the dynamic process, while the intensities of the cross peaks first increase with increasing τ_m due to the exchange process and then decay as a result of T_1. EXSY spectra of $tBBP^{\bullet+}$ in D_2SO_4, shown in Figure 8, display cross peaks between hyperfine components for which $\Delta M_{Ia} = \pm 1$, substantiating our earlier conclusion that they correspond to a change in the spin state of one aromatic proton.

The cross peak patterns in the 2D spectra of the cation radical in H_2SO_4 and D_2SO_4 indicate that the process causing the mixing within the quintet of the aromatic protons is nuclear spin−lattice relaxation whereas that leading to cross peaks within the hydroxyl protons triplets is either nuclear relaxation and/or proton exchange. In order to unambiguously determined the mechanism responsible for the magnetization transfer, the temperature dependence of the cross peaks had to be considered. The 2D spectra recorded at 283 and 310 K with $\tau_m = 1.5$ μs, presented in Figure 9, showed that the relative intensities of the cross peaks decreased considerably with increasing temperature. If the mechanism leading to the exchange were solely proton exchange, then the intensities of the cross peaks should have increased with the temperature due to the increase in the reaction rate. The experiment exhibited the opposite trend. Therefore, we concluded that the cross peaks were generated primarily by nuclear spin−lattice relaxation of the hydroxyl protons, as in the case of the aromatic protons.

Determination of the Nuclear Relaxation Rates. The measured 2D signal is given by[25,26]

$$S(t_1,\tau_m,t_2) = \sum_{ij} S_{ij}(t_1,\tau_m,t_2) = \sum_{ij} P_j(0) A_{ij}(\tau_m) e^{(i\omega_j - 1/T_{2j})t_1} e^{(i\omega_i - 1/T_{2i})t_2} \quad (3)$$

where the indices i, j run over all hyperfine lines. Terms due to axial peaks, which are eliminated by the phase cycle, were not included in eq 3. The $S_{ij}(t_1,\tau_m,t_2)$ terms correspond to cross peaks when $i \neq j$ and to diagonal peaks when $i = j$. $P_j(0)$ is the relative intensity of the jth hyperfine line, and $A_{ij}(\tau_m)$ is the so-called mixing coefficient, given by

$$A_{ij}(\tau_m) = (e^{-\mathbf{R}\tau_m})_{ij} = \sum_k D_{ik} e^{\mathbf{\Lambda}_{kk}\tau_m} D_{kj}^{-1} \quad (4)$$

R is the exchange matrix that includes the relaxation and chemical exchange rates. It is a square matrix, the diagonal elements of which are $R_{ii} = T_{1,i}^{-1} + \sum_j k_{ij}$ and the off-diagonal elements are $R_{ij} = -k_{ij}$, where k_{ij} is the probability of exchange from state j to state i. In our particular case, these are the nuclear relaxation rates of the hydroxyl and aromatic protons, $T_{1b}^{-1} = K_b$ and $T_{1a}^{-1} = K_a$, respectively. The complete **R** matrix is given in Table 4. When there is no exchange, **R** reduces to the electron spin−lattice relaxation times. **Λ** is a diagonal matrix consisting of the eigenvalues of **R**, and **D** is the matrix of the corresponding eigenvectors. After the 2D Fourier transforma-

(25) Ernst, R. R.; Bodenhausen, G.; Wokaum, A. *Principles of NMR in one and two dimensions*; Clarendon Press: Oxford, U.K., 1987.
(26) Macura, S.; Ernst, R. R. *Mol. Phys.* **1980**, *41*, 95.

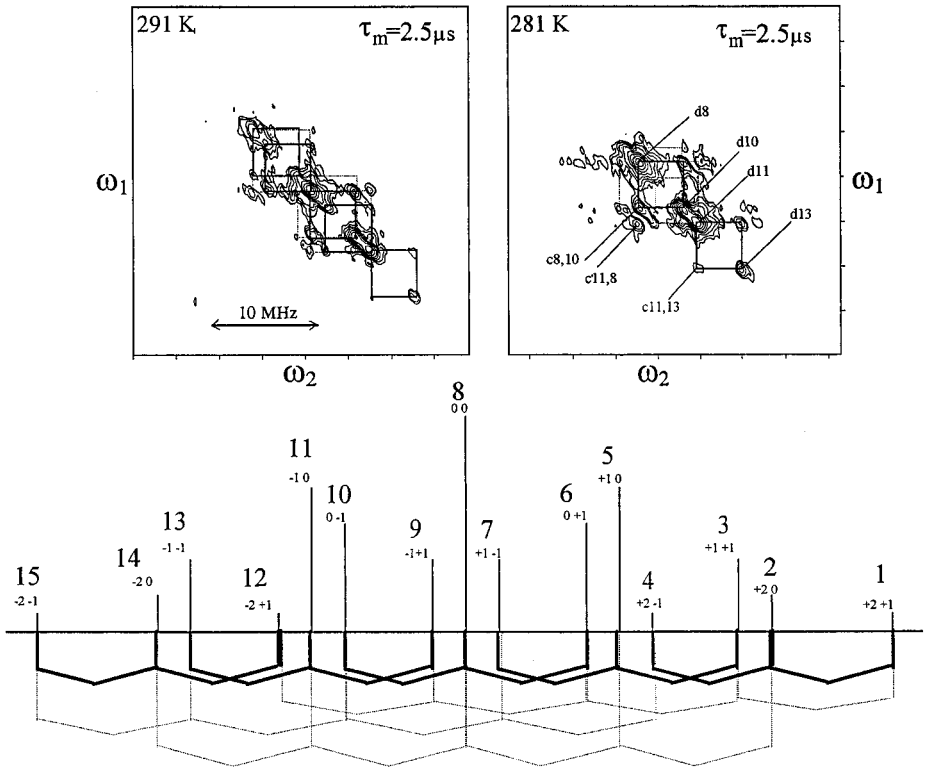

Figure 6. 2D-EXSY spectra of tBBP$^{\bullet+}$ in H_2SO_4 measured at 281 K, 291 K, and τ_m = 2.5 μs. The peaks are marked according to the stick diagram in the lower part of the figure.

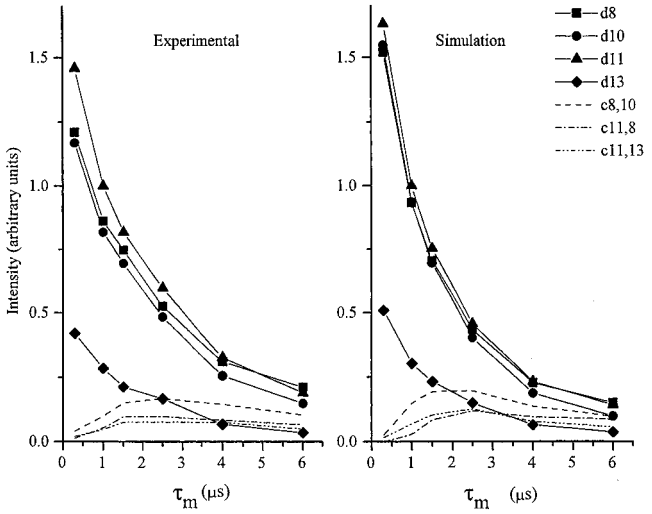

Figure 7. Experimental and simulated curves of the dependence of the amplitudes of the peaks of the 2D spectrum of tBBP$^{\bullet+}$ in H_2SO_4 at 281 K on τ_m.

tion, the intensity of the I_{ij} peak is proportional to $A_{ij}(\tau_m)$. The elements of **R** can be obtained either by simulating the 2D spectrum using eq 3 or by fitting the curves of the peaks intensities vs τ_m using eq 4.[25]

Simulations of the experimental 2D spectra have to take into account the different width of the hyperfine components, the decrease in the radical concentration during the experiment, the spectrometer dead time, and the spectrometer bandwidth. In the 2D experiment, which consist of three pulses, the attenuation of the peak intensities due to the limited spectrometer bandwidth goes as the cube of the attenuation of a single-pulse FT-EPR spectrum. The line widths used in the simulations were obtained from eq 1 using the coefficients listed in Table 3 or extrapolated from Figure 3. Figure 5b shows the best-fit simulated 2D spectra, for 291 K, obtained after taking all the effects listed above into account. The best-fit spectra were chosen by comparing calculated and experimental 2D spectra, until a best visual fit was obtained. The best-fit parameters so obtained for 281 and 291 K are listed in Table 5, and the corresponding intensity curves of the various peaks of the simulated 2D spectra at 281 K are shown in Figure 7.

2D EXSY Measurements of DQ$^{\bullet+}$. The spectrum of DQ$^{\bullet+}$ in H_2SO_4 at 311 K exhibits 39 lines due to splitting by 12 equivalent methyl protons (13 lines) and two hydroxyl protons. The cis−trans isomerization of the hydroxyl groups is fast at 311 K,[27] and therefore, the earlier 2D EXSY experiments were performed at this temperatures.[11] Temperature-dependent 2D EXSY measurements, shown in Figure 10, exhibited cross peaks only within the triplets of the hydroxyl protons. No cross peaks were observed within the methyl group multiplets. The absence of these peaks was further substantiated by measuring the 2D spectrum of DQ$^{\bullet+}$ in D_2SO_4 at 311 K as a function of τ_m. The triplets of the hydroxyl protons were replaced by quintets with a significantly reduced splitting, as expected. No cross peaks were observed between any of the 13 hyperfine components of the methyl protons, indicating that their nuclear spin−lattice relaxation is considerably longer than that of the aromatic protons in tBBP$^{\bullet+}$.

The 2D spectra showed that some of the diagonal peaks broadened with decreasing temperatures because the cis−trans isomerization was no longer fully averaged.[16] Therefore, only peaks that were not broadened by the cis−trans isomerization were considered in the analysis. The amplitudes of these cross peaks relative to the sum of the corresponding two diagonal peaks are listed in Table 6. The relative amplitudes exhibit a small decrease with temperature rather than an increase. This indicates that the cross peaks do not arise only from proton exchange as reported earlier,[11] but that there is a significant contribution from the nuclear relaxation of the hydroxyl protons.

(27) Smith, I. C. P.; Carrington, A. *Mol. Phys.* **1967**, *12*, 439.

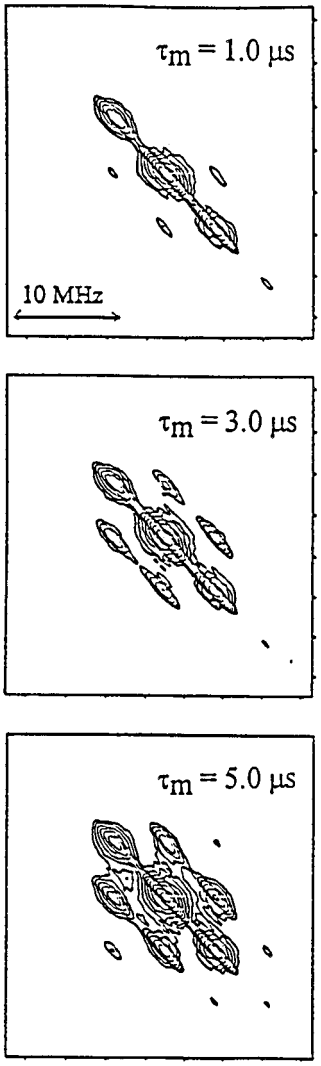

Figure 8. (a) 2D-EXSY contour plots of tBBP$^{\bullet+}$ in D_2SO_4 measured at 291 K, recorded with $\tau_m = 1.0$, 3.0, and 5.0 μs.

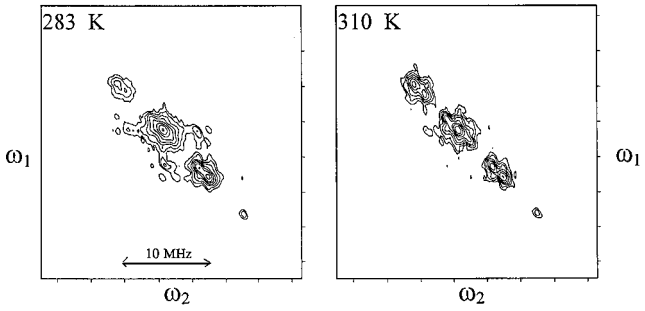

Figure 9. (a) 2D-EXSY contour plot spectra of tBBP$^{\bullet+}$ in H_2SO_4 measured at 283 and 310 K and $\tau_m = 1.5$ μs.

However, in contrast to tBBP$^{\bullet+}$ where the contribution of proton exchange is negligible, in DQ$^{\bullet+}$ both mechanism have significant contributions in the temperature range investigated.

Discussion

The 2D EXSY experiments show that among the dynamic processes leading to the mixing of hyperfine components and therefore to the generation of cross peaks in the 2D spectrum, the nuclear spin lattice relaxation may play a major role. Likewise, in the recent studies of the ordering and dynamic properties of lipid membranes using nitroxide spin labels, cross peaks were observed in the 2D EXSY spectra due to nuclear spin flips induced by the modulation of the hyperfine tensor by the rotational motions.[13,14] Hence, the 2D EXSY method offers an alternative to the CW electron-electron double resonance (ELDOR) method, previously used to measure nuclear relaxation times in radicals.[28,29]

The advantages offered by the 2D exchange method as manifested in this work are the following. (i) The dynamic process could be detected at relatively low temperatures where the radical is more stable. (ii) The mixing mechanism was readily deduced from the pattern of the cross peaks. It was sufficient to measure only a few 2D spectra in order to extract all connectivities and establish that the process involved only $\Delta M_I = \pm 1$ within the different multiplets. (iii) The 2D measurements also gave the electronic T_1, which is not easily determined by CW measurements. Furthermore, it was demonstrated that 2D EXSY is not limited to systems with small spectral width and narrow lines. In spite of the relatively broad EPR lines which make the FT-EPR spectrum most susceptible to the spectrometer dead time, the 2D EXSY method turned out to be efficient both qualitatively and quantitatively. This was also demonstrated in the study of the dynamics of nitroxide spin labels in membranes.[13,14]

In the following we use the nuclear relaxation times determined from the 2D EXSY experiments to calculate the molecular correlation time, τ_c, and show that the relatively large τ_c is consistent with the observed variations of the line width through out the EPR spectrum.

The proton spin−lattice relaxation rate, T_{1N}^{-1}, is given by[30]

$$T_{1N}^{-1} = \frac{\pi^2}{10}\mathrm{Tr}(\mathbf{A}'^2)\frac{\tau_c}{1+\omega_N^2\tau_c^2} \qquad (5)$$

assuming that the prevalent relaxation mechanism is the modulation of the anisotropic hyperfine interaction. At ∼3200 G, $\omega_N^2\tau_c^2 \ll 1$ and T_{1N}^{-1} becomes

$$T_{1N}^{-1} = \frac{\pi}{10}\mathrm{Tr}(\mathbf{A}'^2)\tau_c \qquad (6)$$

$\mathrm{Tr}(\mathbf{A}'^2)$ is given by

$$\mathrm{Tr}(\mathbf{A}'^2) = (A'^2_{XX} + A'^2_{YY} + A'^2_{ZZ}) \qquad (7)$$

where the A'_{ii} correspond to the principal components of the anisotropic hyperfine interaction and are best determined from ENDOR measurements. Unfortunately, such data are not available for tBBP$^{\bullet+}$. Nevertheless, estimates for $\mathrm{Tr}(\mathbf{A}'^2)$ of the ring protons can be obtained from the theory of McConnell and Stradthee.[24,31] According to this theory, the principal components of the dipolar interaction of a proton in a CH fragment in an aromatic radical are

$$A'_{ZZ} = 15.38\rho_\pi, \quad A'_{YY} = -13.64\rho_\pi, \quad A'_{XX} = -1.74\rho_\pi \qquad (8)$$

The A'_{ii} in eq 8 are given in gauss, ρ_π represents the π electron density, and the σ contributions were neglected. The Z axis in eq 8 was taken along the C−H axis, and the X axis was taken along the bisector of the C−C−C angle.[31] ρ_π can be determined from the hyperfine coupling of the aromatic protons using the McConnell relation. Taking $Q = -23$ G, we obtained

(28) Hyde, J. S.; Fronsize, W.; Mottley, C. *Chem. Phys. Lett.* **1984**, *110*, 621.
(29) Maresch, G. G.; Weber, M.; Dubinskii, A. A.; Spiess, H. W. *Chem. Phys. Lett.* **1992**, *193*, 134.
(30) Kurreck, H.; Kirste, B.; Lubitz, W. *Electron Nuclear Double Resonance Spectroscopy of Radicals in solution*; VCH: New York, 1988.
(31) McConnell, H. M.; Strathdee, J. *Mol. Phys.* **1959**, *2*, 129.

Table 4. Exchange Matrix **R** of $tBBP^{\bullet+}$ in H_2SO_4

	2 1	2 0	1 1	2 −1	1 0	0 1	1 −1	0 0	−1 1	0 −1	−1 0	−2 1	−1 −1	−2 0	−2 −1
2 1	$-{}^{2}/_{4}K_b - {}^{4}/_{16}K_a - {}^{1}/_{T1}$	${}^{1}/_{4}K_b$	${}^{1}/_{16}K_a$	0	0	0	0	0	0	0	0	0	0	0	0
2 0	${}^{2}/_{4}K_b$	$-{}^{2}/_{4}K_b - {}^{8}/_{32}K_a - {}^{1}/T_1$	0	${}^{2}/_{4}K_b$	${}^{2}/_{32}K_a$	0	0	0	0	0	0	0	0	0	0
1 1	${}^{4}/_{16}K_a$	0	$-{}^{8}/_{16}K_b - {}^{4}/_{16}K_a - {}^{1}/_{T_1}$	0	${}^{4}/_{16}K_b$	${}^{2}/_{16}K_a$	0	0	0	0	0	0	0	0	0
2 −1	0	${}^{1}/_{4}K_b$	0	$-{}^{2}/_{4}K_b - {}^{4}/_{16}K_a - {}^{1}/_{T_1}$	0	0	$-{}^{1}/_{16}K_a$	0	0	0	0	0	0	0	0
1 0	0	${}^{8}/_{32}K_a$	${}^{8}/_{16}K_b$	0	$-{}^{8}/_{16}K_b - {}^{8}/_{32}K_a - {}^{1}/_{T_1}$	0	${}^{8}/_{16}K_b$	${}^{4}/_{32}K_a$	0	0	0	0	0	0	0
0 1	0	0	${}^{3}/_{16}K_a$	0	0	$-{}^{12}/_{24}K_b - {}^{4}/_{16}K_a - {}^{1}/_{T_1}$	0	${}^{6}/_{24}K_b$	${}^{3}/_{16}K_a$	0	0	0	0	0	0
1 −1	0	0	0	${}^{4}/_{16}K_a$	${}^{4}/_{16}K_b$	0	$-{}^{8}/_{16}K_b - {}^{4}/_{16}K_a - {}^{1}/_{T_1}$	0	0	${}^{2}/_{16}K_a$	0	0	0	0	0
0 0	0	0	0	0	${}^{6}/_{32}K_a$	${}^{12}/_{24}K_b$	0	$-{}^{12}/_{24}K_b - {}^{8}/_{32}K_a - {}^{1}/_{T_1}$	0	${}^{12}/_{24}K_b$	${}^{6}/_{32}K_a$	0	0	0	0
−1 1	0	0 2	0	0	0	${}^{2}/_{16}K_a$	0	0	$-{}^{8}/_{16}K_b - {}^{4}/_{16}K_a - {}^{1}/_{T_1}$	0	${}^{4}/_{16}K_b$	${}^{4}/_{16}K_a$	0	0	0
0 −1	0	0	0	0	0	0	${}^{3}/_{16}K_a$	${}^{6}/_{24}K_b$	0	$-{}^{12}/_{24}K_b - {}^{4}/_{16}K_a - {}^{1}/_{T_1}$	0	0	${}^{3}/_{16}K_a$	0	0
−1 0	0	0	0	0	0	0	0	${}^{4}/_{32}K_a$	${}^{8}/_{16}K_b$	0	$-{}^{8}/_{16}K_b - {}^{8}/_{32}K_a - {}^{1}/_{T_1}$	0	${}^{8}/_{16}K_b$	${}^{8}/_{32}K_a$	0
−2 1	0	0	0	0	0	0	0	0	${}^{1}/_{16}K_a$	0	0	$-{}^{2}/_{4}K_b - {}^{4}/_{16}K_a - {}^{1}/_{T_1}$	0	${}^{1}/_{4}K_b$	0
−1 −1	0	0	0	0	0	0	0	0	0	${}^{2}/_{16}K_a$	${}^{4}/_{16}K_b$	0	$-{}^{8}/_{16}K_b - {}^{4}/_{16}K_a - {}^{1}/_{T_1}$	0	${}^{4}/_{16}K_a$
−2 0	0	0	0	0	0	0	0	0	0	0	${}^{2}/_{32}K_a$	${}^{2}/_{4}K_b$	0	$-{}^{2}/_{4}K_b - {}^{8}/_{32}K_a - {}^{1}/_{T1}$	${}^{2}/_{4}K_b$
−2 −1	0	0	0	0	0	0	0	0	0	0	0	0	${}^{1}/_{16}K_a$	${}^{1}/_{4}K_b$	$-{}^{2}/_{4}K_b - {}^{4}/_{32}K_a - {}^{1}/_{T_1}$

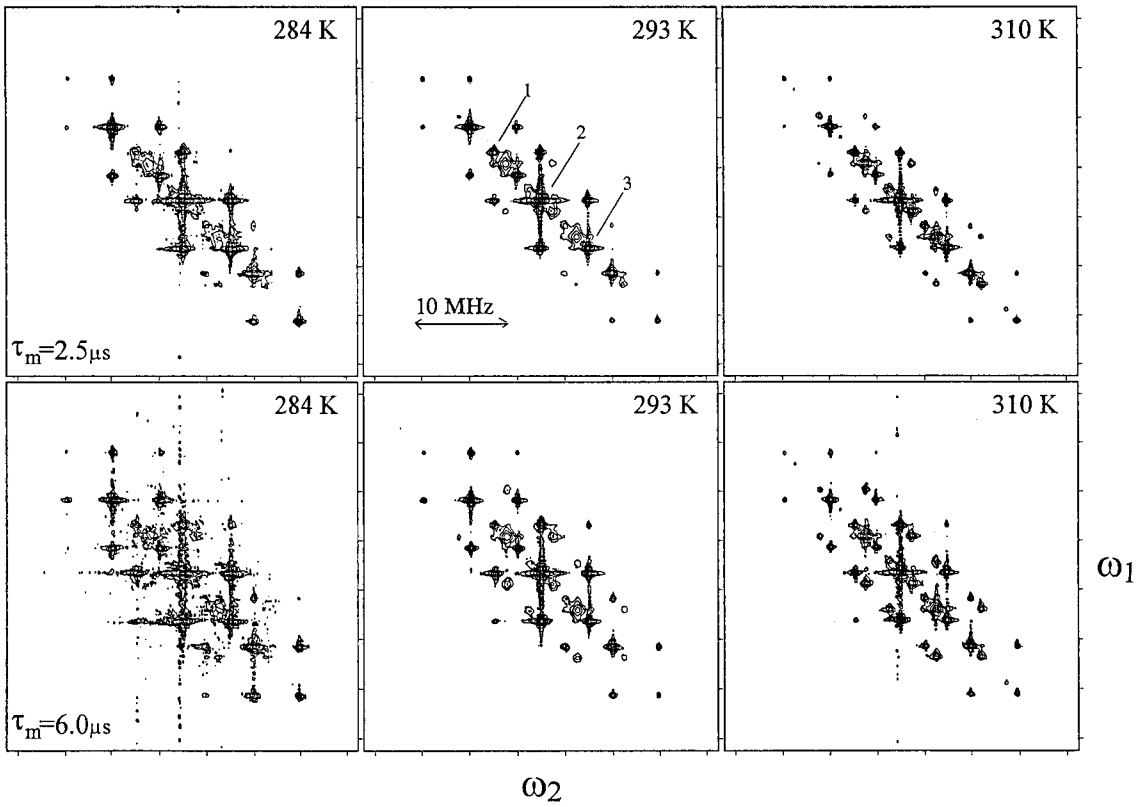

Figure 10. (a) 2D-EXSY contour plot spectra of $DQ^{\bullet+}$ in H_2SO_4 measured at 284, 293, and 310 K and $\tau_m = 2.5$ and 6.0 μs.

Table 5. Best-Fit Simulation Parameters for $tBBP^{\bullet+}$ in H_2SO_4 at 291 and 281K

	281 K (10^{-5} s^{-1})	291 K (10^{-5} s^{-1})
K_a (ring protons)	12 ± 1	9 ± 1
K_b (hydroxyl protons)	7 ± 1	4 ± 1
$(T_1)^{-1}$	1.1 ± 0.1	0.83 ± 0.06

Table 6. Temperature Dependence of the Ratio of the Amplitudes of Cross Peaks (1, 2) and (2, 3) and the Corresponding Diagonal Peaks in the 2D Spectra of $DQ^{\bullet+}$[a]

temp (K)	τ_m (μs)	$\frac{(1,2)}{1+2}$	$\frac{(2,3)}{2+3}$
284	2.5	0.11	0.21
	6	0.18	0.38
293	2.5	0.1	0.17
	6	0.19	0.32
310	2.5	0.09	0.14
	6	0.19	0.27

[a] The peaks are labeled as indicated in Figure 10.

$\rho_\pi(C_a) = 0.078$ and $Tr(\mathbf{A}'^2) = 8.04 \times 10^{14}$ s^{-2}. Substitution of these values in eq 6 yields $\tau_c = 1.5 \times 10^{-9}$ s and $\tau_c = 1.1 \times 10^{-9}$ s at 281 and 291 K, respectively.

An estimate for $Tr(\mathbf{A}')^2$ can also be obtained from the dipolar tensor of *p*-benzoquinone radical anion measured by ENDOR or high-field EPR.[32] Assuming that the *Q* values of the protons in both anion and cation radicals are close,[33] the A'_{ii} values of the *p*-benzoquinone radical can be used for $tBBP^{\bullet+}$ after the appropriate scaling accounting for the different spin densities on the aromatic protons. The isotropic hyperfine constant of the aromatic protons in the *p*-benzoquinone radical anion is 2.35 G compared to 1.81 G in $tBBP^{\bullet+}$; hence we scaled down the anisotropic hyperfine of the *p*-benzoquinone radical by a factor of 1.81/2.35 and obtained $A'_{ZZ} = -1.92$ MHz, $A'_{XX} = -2.77$ MHz, and $A'_{YY} = 4.77$ MHz. These values yield $Tr(\mathbf{A}'^2) = 13.4 \times 10^{14}$ s^{-2} and τ_c values of 0.9×10^{-9} s and 0.67×10^{-9} s at 281 and 291 K, respectively. These values are close to those obtained using the theory of McConnell and Stradthee[31] and can provide the uncertainty range for τ_c. The relatively high value of τ_c is not surprising considering the high viscosity of concentrated sulfuric acid.

Table 7. Hyperfine Coupling Constant of the Hydroxyl Protons and HMO Spin Populations in Semiquinone Radical Cations

compound	ρ_π(O)	*a* (G)	ref
p-benzoquinone	0.1786[b]	3.44	34
p-benzoquinone	0.113[b]	3.44[a]	35
naphthoquinone	0.079[b]	2.42	35
anthraquinone	0.065[a]	1.32	35
anthraquinone	0.055[b]		35

[a] Experimental. [b] Simulation.

Using eq 6 and the correlation time obtained from the ring protons ($\tau_c = 1.5 \times 10^{-9}$ s, at 281 K), $Tr(\mathbf{A}'^2)$ of the hydroxyl protons was evaluated to be 4.69×10^{14} s^{-2}. Assuming that for the hydroxyl protons the major contribution to $\mathbf{A}'$ arises from the spin density on the oxygen p_z orbital, ρ_π(O), and taking the O−H bond distance to be similar to that of the C−H bond, we get

$$\frac{\rho_\pi^2(O)}{\rho_\pi^2(C_a)} = \frac{Tr(\mathbf{A}'^2)(OH)}{Tr(\mathbf{A}'^2)(aromatic)} = 0.58 \qquad (9)$$

and $\rho_\pi(O) = 0.059$. For comparison, Table 7 lists ρ_π(O) values and hyperfine couplings constants of other quinone cation radicals, which are in a reasonable agreement with the value above.

We now proceed to calculate the coefficients of eq 1, which determines the line width variation. The general theory of line width in the EPR spectrum[23] shows that when the radical has

(32) Burghaus, O.; Plato, M.; Rohrer, M.; Mobius, K.; Macmillan, F. *J. Chem. Phys.* **1993**, *97*, 7639.

(33) Gerson, F. *High Resolution ESR Spectroscopy*; John Wiley and Sons: London, 1970.

two groups of completely equivalent protons, the coefficients in eq 1 are given by[23,24]

$$a = {}^{10}/_{3}[j_a^{(D)}(0)I_a(I_a+1) + j_b^{(D)}I_b(I_b+1)] + C \quad (10)$$

$$b_i = {}^{16}/_{3}B_0 j_i^{(DG_2)}(0) \quad (11)$$

$$c_i = {}^{5}/_{3}j_i^{(D)}(0) \quad (12)$$

$$d = {}^{8}/_{3}j_{ab}^{(D)}(0) \quad (13)$$

where

$$j_i^{(D)}(0) = \frac{1}{5}\tau_c\gamma_i^2\hbar^2[(D_i^{(0)})^2 + 2|D_i^{(2)}|^2] \quad (14)$$

$$j_{ab}^{(D)}(0) = \frac{1}{5}\tau_c\gamma_e^2\gamma_a\gamma_b\hbar^2[D_a^{(0)}D_b^{(0)} + D_a^{(2)}D_b^{(-2)} + D_a^{(-2)}D_b^{(2)}] \quad (15)$$

and

$$j_i^{(DG_2)}(0) = \frac{1}{10}\tau_c\beta_e|\gamma_e|\gamma_i[D_i^{(0)}g^{(0)} + (D_i^{(2)} + D_i^{(-2)})g^{(2)}] \quad (16)$$

The index i corresponds to nuclei in groups a or b and C includes terms not related to the anisotropic parts of **g** and **A**. $D_i^{(0)}$ and $D_i^{(\pm 2)}$ are the irreducible tensor components of the dipolar interaction of the nuclei in group i. The parameters $g^{(0)}$ and $g^{(2)}$ are related to the anisotropy of the g tensor and its deviation from axial symmetry, respectively, as follows:[23]

$$g^{(0)} = 6^{-1/2}[2g_3 - (g_1 + g_2)] \quad (17)$$

$$g^{(\pm 2)} = ({}^{1}/_{2})[g_1 - g_2]$$

$$g_1 = g_{xx}, \quad g_2 = g_{yy}, \quad g_3 = g_{zz}$$

In the derivation of eqs 11−13, secular and pseudosecular terms were taken into account whereas nonsecular terms were neglected since $(\omega_e\tau_c)^2 \gg 1$.[23] Any possible contribution of the modulation of the isotropic hyperfine constant, which may be induced by the cis−trans isomerization process, to the line width variation[23] has been neglected in the above.

The components of the anisotropic hyperfine tensor, $D_i^{(m)}$, are given by the sum of the proton dipolar interactions with the unpaired electron density in each of the p_π orbitals in the molecule according to[23]

$$D_i^{(0)} = -\left(\frac{1}{2}\right)\left(\frac{3}{2}\right)^{1/2}\sum_k \rho_\pi(k)d_{k,3} \quad (18)$$

$$D_i^{(\pm 2)} = {}^{1}/_{4}\sum_k \rho_\pi(k)(d_{k,2} - d_{k,1})e^{\mp 2i\alpha_k} \quad (19)$$

$\rho_\pi(k)$ is the unpaired spin density in the p_π orbital on atom k, and the $d_{k,n}$ ($n = 1, 2, 3$) are the principle values of the dipolar tensor between the electron in the p_π orbital of atom k and the nucleus of interest. α_k is the angle between the the vector connecting the proton and the k atom and the g_{xx} direction. Contributions from the spin density in σ orbitals have been neglected in eqs 18 and 19. Neglecting contributions from distant carbons, we took only $k = 1$. As mentioned earlier, specific expressions for the $d_{1,n}$ can be obtained from the theory of McConnell and Strathdee[24,31] according to

$$A'_{ZZ} = d_{1,2}, A'_{XX} = d_{1,3}, A'_{YY} = d_{1,1} \quad (20)$$

The expressions for the $d_{1,n}$ (eqs 18 and 19) were given with respect to the principal axis system of **g**[23] whereas McConnell's expression was derived using an axis system where Z is along the C−H bond. These different axes definitions were taken into account in eq 20.

The coefficient c_a (see eq 1) of the ring protons can be calculated using the principal values of **A′** of the aromatic protons calculated earlier. Using eqs 18−20 and $\rho_\pi(C_a) = 0.078$ we obtained $(D_a^{(0)})^2 = 2.13 \times 10^{12}$ s^{-2} and $|D_a^{(\pm 2)}|^2 = 1.0 \times 10^{14}$ s^{-2}. After substituting these values into eqs 12 and 14 and taking $\tau_c = 1.5 \times 10^{-9}$ s (281 K), $c_a = 1.0 \times 10^5$ s^{-1} is obtained. Considering the approximations made and the experimental uncertainties (see Figure 3), this is a surprisingly good agreement with the experimental values, 1.3×10^5 s^{-1}.

The g-anisotropy, $\Delta g = g_3 - {}^{1}/_{2}(g_1 + g_2)$, can be estimated from eqs 11 and 16 using the experimentally determined b_a coefficient (Table 3), τ_c, and the $D_a^{(0)}$ and $D_a^{(\pm 2)}$ values given above. It is not possible to deduce the three principal values of the **g** tensor from the experimental results and therefore the biaxiality contribution, which is expected to be small,[24] has been neglected. In this case, eq 16 reduces to

$$J_i^{(DG)_2} = {}^{1}/_{10}\tau_c|\gamma_e|\beta_e\gamma_i D^{(0)}g^{(0)} \quad (21)$$

This calculation gave $g^{(0)} = -0.028$ and $\Delta g = -0.034$. This value is larger than values of Δg reported in the literature. For instance, Δg of the *p*-benzoquinone cation radical was estimated by a similar method to be -2.9×10^{-3}.[24] High-field EPR measurements on a series of quinone anion radicals gave values of Δg in the range of -5.2×10^{-3} to -7.4×10^{-3}.[32]

In this work the nuclear relaxation rate was first determined by the 2D EXSY method, and then, using the appropriate line width theory, the correlation time, which was extracted from the relaxation rate, was shown to be compatible with the observed line width variation in the EPR spectrum. It is, however, possible to use a more general theory for the analysis of the 2D spectra which includes the line width variation. Such a general approach, based on the stochastic Liouville equation, was used in the investigation of the dynamics of nitroxide spin labels in membranes, where the 2D simulations provided both the line width variation and the cross peak development.[13,14] This approach requires the knowledge of **A** and **g**. We preferred to carry out the analysis in two stages primarily because of the many assumptions we had to make to estimate the hyperfine tensors of the various protons and the g tensor of the radical, which were unknown. These parameters were essential for the second stage but not for the first.

We finally discuss the implications of the faster proton exchange in $DQ^{\bullet+}$ as compared to $tBBP^{\bullet+}$. In general, two possible mechanisms for proton exchange can be considered. In mechanism I, the initial step consists of the protonation of the hydroxyl group, which is then followed by a proton release. The initial step of mechanism II is the release of the hydroxyl proton to yield a semiquinone radical type and then protonation takes place. The rates of these two mechanisms are affected by the negative charge on the oxygen in opposite ways. While a larger negative charge will cause an increase in the rate of mechanism I it will result in a decrease in the rate of mechanism II. Hence, a comparison of the relative effective charge on the oxygens in $tBBP^{\bullet+}$ and $DQ^{\bullet+}$, combined with the experimental observation, may suggest which is the preferred mechanism. The effective charges on the oxygens were estimated from ab initio UHF quantum chemical calculations (using the 6-31G[36] basis set with full optimization of the geometry) on the trans

(34) Vincow, G.; Frankel, G. K. *J. Chem. Phys.* **1961**, *54*, 1333.

configuration of 4,4′-dihydroxydiphenyl and the dihydroquinone radical cations, which are structurally related to $tBBP^{\bullet+}$ and $DQ^{\bullet+}$. In doing so we assumed that the effect of the methyl groups in $DQ^{\bullet+}$ and the *tert*-butyl groups in $tBBP^{\bullet+}$ on the effective charge distribution is approximately the same. These calculations showed that the negative charge on the oxygens of the dihydroquinone radical cation was smaller (−0.654) than in the 4,4′-dihydroxydiphenyl radical cation (−0.698). This suggests that the former should be more acidic and less basic than the latter, and therefore, a faster proton exchange is indeed expected for $DQ^{\bullet+}$ if the proton exchange occurs according to mechanism II. In the above discussion possible steric effects of the larger *tert*-butyl groups were not taken into account. It seems, though, that mechanism I would be more sensitive to steric effects than mechanism II.

Conclusions

The nuclear spin−lattice relaxation rates of both the aromatic and hydroxyl protons in the 1,1′-dihydroxy-2,2′,6,6′-tetra-*tert*-butylbiphenyl cation radical in sulfuric acid are relatively fast due to the high viscosity of the solution and therefore lead to the generation of cross peaks in the 2D EXSY spectrum. Since the exchange of the hydroxyl protons with the solvent and their nuclear spin−lattice relaxation produce the same cross-peak pattern, it is essential to carry out temperature-dependent measurements in order to distinguish between the two processes. The proton exchange in $DQ^{\bullet+}$ was found to be faster than in $tBBP^{\bullet+}$.

Acknowledgment. This study was made possible by Grant 90-00128 from the United States−Israel Binational Science Foundation, Jerusalem. We thank Prof. Z. Luz and Dr. M. K. Bowman for many helpful discussions.

JA960737H

(35) Carrington, A.; Bolton, J. R.; Santos-Veiga, J. *Mol. Phys.* **1962**, *5*, 465.

(36) Gaussian 94 (Revision C2). Frisch, M. J.; Trucks, G. W.; Schlegel, H. B.; Gill, P. M. W.; Johnson, B. G.; Robb, M. A.; Cheeseman, J. R.; Keith, T. A.; Patersson, G. A.; Motgomery, J. A.; Raghavachari, K.; Al-Laham, M. A.; Zakrzewski, V. G.; Ortiz, J. V.; Foresman, J. B.; Cioslowski, J.; Stefanov, B.; Nanayakkara, A.; Challacombe, M.; Peng, C. Y.; Ayala, P. Y.; Chen, W.; Wong, M. W.; Andres, J. L.; Replogle, E. S.; Gomperts, R.; Martin, R. L.; Fox, D. J.; Binkley, J. S.; Defrees, D. J.; Baker, J.; Stewart, J. P.; Head-Gordon, M.; Gonzalez, C.; Pople, J. H., Gaussian, Inc., Pittsburgh, PA, 1995.